

Evidence for $Z_c(3900)^\pm$ decays into the $\rho^\pm\eta_c$ final state

M. Ablikim¹, M. N. Achasov^{10,d}, S. Ahmed¹⁵, M. Albrecht⁴, M. Alekseev^{55A,55C}, A. Amoroso^{55A,55C}, F. F. An¹, Q. An^{52,42}, Y. Bai⁴¹, O. Bakina²⁷, R. Baldini Ferroli^{23A}, Y. Ban³⁵, K. Begzsuren²⁵, D. W. Bennett²², J. V. Bennett⁵, N. Berger²⁶, M. Bertani^{23A}, D. Bettoni^{24A}, F. Bianchi^{55A,55C}, E. Boger^{27,b}, I. Boyko²⁷, R. A. Briere⁵, H. Cai⁵⁷, X. Cai^{1,42}, A. Calcaterra^{23A}, G. F. Cao^{1,46}, S. A. Cetin^{45B}, J. Chai^{55C}, J. F. Chang^{1,42}, W. L. Chang^{1,46}, G. Chelkov^{27,b,c}, G. Chen¹, H. S. Chen^{1,46}, J. C. Chen¹, M. L. Chen^{1,42}, P. L. Chen⁵³, S. J. Chen³³, X. R. Chen³⁰, Y. B. Chen^{1,42}, W. Cheng^{55C}, X. K. Chu³⁵, G. Cibinetto^{24A}, F. Cossio^{55C}, H. L. Dai^{1,42}, J. P. Dai^{37,h}, A. Dbeysi¹⁵, D. Dedovich²⁷, Z. Y. Deng¹, A. Denig²⁶, I. Denysenko²⁷, M. Destefanis^{55A,55C}, F. De Mori^{55A,55C}, Y. Ding³¹, C. Dong³⁴, J. Dong^{1,42}, L. Y. Dong^{1,46}, M. Y. Dong^{1,42,46}, Z. L. Dou³³, S. X. Du⁶⁰, P. F. Duan¹, J. Fang^{1,42}, S. S. Fang^{1,46}, Y. Fang¹, R. Farinelli^{24A,24B}, L. Fava^{55B,55C}, F. Feldbauer⁴, G. Felici^{23A}, C. Q. Feng^{52,42}, M. Fritsch⁴, C. D. Fu¹, Q. Gao¹, X. L. Gao^{52,42}, Y. Gao⁴⁴, Y. G. Gao⁶, Z. Gao^{52,42}, B. Garillon²⁶, I. Garzia^{24A}, A. Gilman⁴⁹, K. Goetzen¹¹, L. Gong³⁴, W. X. Gong^{1,42}, W. Gradl²⁶, M. Greco^{55A,55C}, L. M. Gu³³, M. H. Gu^{1,42}, Y. T. Gu¹³, A. Q. Guo^{1,22}, L. B. Guo³², R. P. Guo^{1,46}, Y. P. Guo²⁶, A. Guskov²⁷, Z. Haddadi²⁹, S. Han⁵⁷, X. Q. Hao¹⁶, F. A. Harris⁴⁷, K. L. He^{1,46}, F. H. Heinsius⁴, T. Held⁴, Y. K. Heng^{1,42,46}, Z. L. Hou¹, H. M. Hu^{1,46}, J. F. Hu^{37,h}, T. Hu^{1,42,46}, Y. Hu¹, G. S. Huang^{52,42}, J. S. Huang¹⁶, X. T. Huang³⁶, X. Z. Huang³³, Z. L. Huang³¹, T. Hussain⁵⁴, W. Ikegami Andersson⁵⁶, M. Irshad^{52,42}, Q. Ji¹, Q. P. Ji¹⁶, X. B. Ji^{1,46}, X. L. Ji^{1,42}, H. L. Jiang³⁶, X. S. Jiang^{1,42,46}, X. Y. Jiang³⁴, J. B. Jiao³⁶, Z. Jiao¹⁸, D. P. Jin^{1,42,46}, S. Jin³³, Y. Jin⁴⁸, T. Johansson⁵⁶, A. Julin⁴⁹, N. Kalantar-Nayestanaki²⁹, X. S. Kang³⁴, M. Kavatsyuk²⁹, B. C. Ke¹, I. K. Keshk⁴, T. Khan^{52,42}, A. Khoukaz⁵⁰, P. Kiese²⁶, R. Kiuchi¹, R. Kliemt¹¹, L. Koch²⁸, O. B. Kolcu^{45B,f}, B. Kopf⁴, M. Kuemmel⁴, M. Kuessner⁴, A. Kupsc⁵⁶, M. Kurth¹, W. Kühn²⁸, J. S. Lange²⁸, P. Larin¹⁵, L. Lavezzi^{55C}, S. Leiber⁴, H. Leithoff²⁶, C. Li⁵⁶, Cheng Li^{52,42}, D. M. Li⁶⁰, F. Li^{1,42}, F. Y. Li³⁵, G. Li¹, H. B. Li^{1,46}, H. J. Li^{1,46}, J. C. Li¹, J. W. Li⁴⁰, K. J. Li⁴³, Kang Li¹⁴, Ke Li¹, Lei Li³, P. L. Li^{52,42}, P. R. Li^{46,7}, Q. Y. Li³⁶, T. Li³⁶, W. D. Li^{1,46}, W. G. Li¹, X. L. Li³⁶, X. N. Li^{1,42}, X. Q. Li³⁴, Z. B. Li⁴³, H. Liang^{52,42}, Y. F. Liang³⁹, Y. T. Liang²⁸, G. R. Liao¹², L. Z. Liao^{1,46}, J. Libby²¹, C. X. Lin⁴³, D. X. Lin¹⁵, B. Liu^{37,h}, B. J. Liu¹, C. X. Liu¹, D. Liu^{52,42}, D. Y. Liu^{37,h}, F. H. Liu³⁸, Fang Liu¹, Feng Liu⁶, H. B. Liu¹³, H. L. Liu⁴¹, H. M. Liu^{1,46}, Huanhuan Liu¹, Huihui Liu¹⁷, J. B. Liu^{52,42}, J. Y. Liu^{1,46}, K. Y. Liu³¹, Ke Liu⁶, L. D. Liu³⁵, Q. Liu⁴⁶, S. B. Liu^{52,42}, X. Liu³⁰, Y. B. Liu³⁴, Z. A. Liu^{1,42,46}, Zhiqing Liu²⁶, Y. F. Long³⁵, X. C. Lou^{1,42,46}, H. J. Lu¹⁸, J. G. Lu^{1,42}, Y. Lu¹, Y. P. Lu^{1,42}, C. L. Luo³², M. X. Luo⁵⁹, P. W. Luo⁴³, T. Luo^{9,j}, X. L. Luo^{1,42}, S. Lusso^{55C}, X. R. Lyu⁴⁶, F. C. Ma³¹, H. L. Ma¹, L. L. Ma³⁶, M. M. Ma^{1,46}, Q. M. Ma¹, X. N. Ma³⁴, X. Y. Ma^{1,42}, Y. M. Ma³⁶, F. E. Maas¹⁵, M. Maggiora^{55A,55C}, S. Maldaner²⁶, Q. A. Malik⁵⁴, A. Mangoni^{23B}, Y. J. Mao³⁵, Z. P. Mao¹, S. Marcello^{55A,55C}, Z. X. Meng⁴⁸, J. G. Messchendorp²⁹, G. Mezzadri^{24A}, J. Min^{1,42}, T. J. Min³³, R. E. Mitchell²², X. H. Mo^{1,42,46}, Y. J. Mo⁶, C. Morales Morales¹⁵, N. Yu. Muchnoi^{10,d}, H. Muramatsu⁴⁹, A. Mustafa⁴, S. Nakhoul^{11,g}, Y. Nefedov²⁷, F. Nerling^{11,g}, I. B. Nikolaev^{10,d}, Z. Ning^{1,42}, S. Nisar⁸, S. L. Niu^{1,42}, X. Y. Niu^{1,46}, S. L. Olsen⁴⁶, Q. Ouyang^{1,42,46}, S. Pacetti^{23B}, Y. Pan^{52,42}, M. Papenbrock⁵⁶, P. Patteri^{23A}, M. Pelizaeus⁴, J. Pellegrino^{55A,55C}, H. P. Peng^{52,42}, Z. Y. Peng¹³, K. Peters^{11,g}, J. Pettersson⁵⁶, J. L. Ping³², R. G. Ping^{1,46}, A. Pitka⁴, R. Poling⁴⁹, V. Prasad^{52,42}, H. R. Qi², M. Qi³³, T. Y. Qi², S. Qian^{1,42}, C. F. Qiao⁴⁶, N. Qin⁵⁷, X. S. Qin⁴, Z. H. Qin^{1,42}, J. F. Qiu¹, S. Q. Qu³⁴, K. H. Rashid^{54,i}, C. F. Redmer²⁶, M. Richter⁴, M. Ripka²⁶, A. Rivetti^{55C}, M. Rolo^{55C}, G. Rong^{1,46}, Ch. Rosner¹⁵, A. Sarantsev^{27,e}, M. Savrie^{24B}, K. Schoenning⁵⁶, W. Shan¹⁹, X. Y. Shan^{52,42}, M. Shao^{52,42}, C. P. Shen², P. X. Shen³⁴, X. Y. Shen^{1,46}, H. Y. Sheng¹, X. Shi^{1,42}, J. J. Song³⁶, W. M. Song³⁶, X. Y. Song¹, S. Sosio^{55A,55C}, C. Sowa⁴, S. Spataro^{55A,55C}, F. F. Sui³⁶, G. X. Sun¹, J. F. Sun¹⁶, L. Sun⁵⁷, S. S. Sun^{1,46}, X. H. Sun¹, Y. J. Sun^{52,42}, Y. K. Sun^{52,42}, Y. Z. Sun¹, Z. J. Sun^{1,42}, Z. T. Sun¹, Y. T. Tan^{52,42}, C. J. Tang³⁹, G. Y. Tang¹, X. Tang¹, M. Tiemens²⁹, B. Tsednee²⁵, I. Uman^{45D}, B. Wang¹, B. L. Wang⁴⁶, C. W. Wang³³, D. Wang³⁵, D. Y. Wang³⁵, Dan Wang⁴⁶, H. H. Wang³⁶, K. Wang^{1,42}, L. L. Wang¹, L. S. Wang¹, M. Wang³⁶, Meng Wang^{1,46}, P. Wang¹, P. L. Wang¹, W. P. Wang^{52,42}, X. F. Wang¹, Y. Wang^{52,42}, Y. F. Wang^{1,42,46}, Z. Wang^{1,42}, Z. G. Wang^{1,42}, Z. Y. Wang¹, Zongyuan Wang^{1,46}, T. Weber⁴, D. H. Wei¹², P. Weidenkaff²⁶, S. P. Wen¹, U. Wiedner⁴, M. Wolke⁵⁶, L. H. Wu¹, L. J. Wu^{1,46}, Z. Wu^{1,42}, L. Xia^{52,42}, X. Xia³⁶, Y. Xia²⁰, D. Xiao¹, Y. J. Xiao^{1,46}, Z. J. Xiao³², Y. G. Xie^{1,42}, Y. H. Xie⁶, X. A. Xiong^{1,46}, Q. L. Xiu^{1,42}, G. F. Xu¹, J. J. Xu^{1,46}, L. Xu¹, Q. J. Xu¹⁴, X. P. Xu⁴⁰, F. Yan⁵³, L. Yan^{55A,55C}, W. B. Yan^{52,42}, W. C. Yan², Y. H. Yan²⁰, H. J. Yang^{37,h}, H. X. Yang¹, L. Yang⁵⁷, R. X. Yang^{52,42}, S. L. Yang^{1,46}, Y. H. Yang³³, Y. X. Yang¹², Yifan Yang^{1,46}, Z. Q. Yang²⁰, M. Ye^{1,42}, M. H. Ye⁷, J. H. Yin¹, Z. Y. You⁴³, B. X. Yu^{1,42,46}, C. X. Yu³⁴, J. S. Yu³⁰, J. S. Yu²⁰, C. Z. Yuan^{1,46}, Y. Yuan¹, A. Yuncu^{45B,a}, A. A. Zafar⁵⁴, Y. Zeng²⁰, B. X. Zhang¹, B. Y. Zhang^{1,42}, C. C. Zhang¹, D. H. Zhang¹, H. H. Zhang⁴³, H. Y. Zhang^{1,42}, J. Zhang^{1,46}, J. L. Zhang⁵⁸, J. Q. Zhang⁴, J. W. Zhang^{1,42,46}, J. Y. Zhang¹, J. Z. Zhang^{1,46}, K. Zhang^{1,46}, L. Zhang⁴⁴, S. F. Zhang³³, T. J. Zhang^{37,h}, X. Y. Zhang³⁶, Y. Zhang^{52,42}, Y. H. Zhang^{1,42}, Y. T. Zhang^{52,42}, Yang Zhang¹, Yao Zhang¹, Yu Zhang⁴⁶, Z. H. Zhang⁶, Z. P. Zhang⁵², Z. Y. Zhang⁵⁷, G. Zhao¹, J. W. Zhao^{1,42}, J. Y. Zhao^{1,46}, J. Z. Zhao^{1,42}, Lei Zhao^{52,42}, Ling Zhao¹,

M. G. Zhao³⁴, Q. Zhao¹, S. J. Zhao⁶⁰, T. C. Zhao¹, Y. B. Zhao^{1,42}, Z. G. Zhao^{52,42}, A. Zhemchugov^{27,b}, B. Zheng⁵³, J. P. Zheng^{1,42}, W. J. Zheng³⁶, Y. H. Zheng⁴⁶, B. Zhong³², L. Zhou^{1,42}, Q. Zhou^{1,46}, X. Zhou⁵⁷, X. K. Zhou^{52,42}, X. R. Zhou^{52,42}, X. Y. Zhou¹, Xiaoyu Zhou²⁰, Xu Zhou²⁰, A. N. Zhu^{1,46}, J. Zhu³⁴, J. Zhu⁴³, K. Zhu¹, K. J. Zhu^{1,42,46}, S. Zhu¹, S. H. Zhu⁵¹, X. L. Zhu⁴⁴, Y. C. Zhu^{52,42}, Y. S. Zhu^{1,46}, Z. A. Zhu^{1,46}, J. Zhuang^{1,42}, B. S. Zou¹, J. H. Zou¹

(BESIII Collaboration)

- ¹ *Institute of High Energy Physics, Beijing 100049, People's Republic of China*
² *Beihang University, Beijing 100191, People's Republic of China*
³ *Beijing Institute of Petrochemical Technology, Beijing 102617, People's Republic of China*
⁴ *Bochum Ruhr-University, D-44780 Bochum, Germany*
⁵ *Carnegie Mellon University, Pittsburgh, Pennsylvania 15213, USA*
⁶ *Central China Normal University, Wuhan 430079, People's Republic of China*
⁷ *China Center of Advanced Science and Technology, Beijing 100190, People's Republic of China*
⁸ *COMSATS Institute of Information Technology, Lahore, Defence Road, Off Raiwind Road, 54000 Lahore, Pakistan*
⁹ *Fudan University, Shanghai 200443, People's Republic of China*
¹⁰ *G.I. Budker Institute of Nuclear Physics SB RAS (BINP), Novosibirsk 630090, Russia*
¹¹ *GSI Helmholtzcentre for Heavy Ion Research GmbH, D-64291 Darmstadt, Germany*
¹² *Guangxi Normal University, Guilin 541004, People's Republic of China*
¹³ *Guangxi University, Nanning 530004, People's Republic of China*
¹⁴ *Hangzhou Normal University, Hangzhou 310036, People's Republic of China*
¹⁵ *Helmholtz Institute Mainz, Johann-Joachim-Becher-Weg 45, D-55099 Mainz, Germany*
¹⁶ *Henan Normal University, Xinxiang 453007, People's Republic of China*
¹⁷ *Henan University of Science and Technology, Luoyang 471003, People's Republic of China*
¹⁸ *Huangshan College, Huangshan 245000, People's Republic of China*
¹⁹ *Hunan Normal University, Changsha 410081, People's Republic of China*
²⁰ *Hunan University, Changsha 410082, People's Republic of China*
²¹ *Indian Institute of Technology Madras, Chennai 600036, India*
²² *Indiana University, Bloomington, Indiana 47405, USA*
²³ *(A)INFN Laboratori Nazionali di Frascati, I-00044, Frascati, Italy; (B)INFN and University of Perugia, I-06100, Perugia, Italy*
²⁴ *(A)INFN Sezione di Ferrara, I-44122, Ferrara, Italy; (B)University of Ferrara, I-44122, Ferrara, Italy*
²⁵ *Institute of Physics and Technology, Peace Ave. 54B, Ulaanbaatar 13330, Mongolia*
²⁶ *Johannes Gutenberg University of Mainz, Johann-Joachim-Becher-Weg 45, D-55099 Mainz, Germany*
²⁷ *Joint Institute for Nuclear Research, 141980 Dubna, Moscow region, Russia*
²⁸ *Justus-Liebig-Universitaet Giessen, II. Physikalisches Institut, Heinrich-Buff-Ring 16, D-35392 Giessen, Germany*
²⁹ *KVI-CART, University of Groningen, NL-9747 AA Groningen, The Netherlands*
³⁰ *Lanzhou University, Lanzhou 730000, People's Republic of China*
³¹ *Liaoning University, Shenyang 110036, People's Republic of China*
³² *Nanjing Normal University, Nanjing 210023, People's Republic of China*
³³ *Nanjing University, Nanjing 210093, People's Republic of China*
³⁴ *Nankai University, Tianjin 300071, People's Republic of China*
³⁵ *Peking University, Beijing 100871, People's Republic of China*
³⁶ *Shandong University, Jinan 250100, People's Republic of China*
³⁷ *Shanghai Jiao Tong University, Shanghai 200240, People's Republic of China*
³⁸ *Shanxi University, Taiyuan 030006, People's Republic of China*
³⁹ *Sichuan University, Chengdu 610064, People's Republic of China*
⁴⁰ *Soochow University, Suzhou 215006, People's Republic of China*
⁴¹ *Southeast University, Nanjing 211100, People's Republic of China*
⁴² *State Key Laboratory of Particle Detection and Electronics, Beijing 100049, Hefei 230026, People's Republic of China*
⁴³ *Sun Yat-Sen University, Guangzhou 510275, People's Republic of China*
⁴⁴ *Tsinghua University, Beijing 100084, People's Republic of China*
⁴⁵ *(A)Ankara University, 06100 Tandogan, Ankara, Turkey; (B)Istanbul Bilgi University, 34060 Eyup, Istanbul, Turkey;*

(C)Uludag University, 16059 Bursa, Turkey; (D)Near East University, Nicosia, North Cyprus, Mersin 10, Turkey

⁴⁶ University of Chinese Academy of Sciences, Beijing 100049, People's Republic of China

⁴⁷ University of Hawaii, Honolulu, Hawaii 96822, USA

⁴⁸ University of Jinan, Jinan 250022, People's Republic of China

⁴⁹ University of Minnesota, Minneapolis, Minnesota 55455, USA

⁵⁰ University of Muenster, Wilhelm-Klemm-Str. 9, 48149 Muenster, Germany

⁵¹ University of Science and Technology Liaoning, Anshan 114051, People's Republic of China

⁵² University of Science and Technology of China, Hefei 230026, People's Republic of China

⁵³ University of South China, Hengyang 421001, People's Republic of China

⁵⁴ University of the Punjab, Lahore-54590, Pakistan

⁵⁵ (A)University of Turin, I-10125, Turin, Italy; (B)University of Eastern Piedmont, I-15121, Alessandria, Italy; (C)INFN, I-10125, Turin, Italy

⁵⁶ Uppsala University, Box 516, SE-75120 Uppsala, Sweden

⁵⁷ Wuhan University, Wuhan 430072, People's Republic of China

⁵⁸ Xinyang Normal University, Xinyang 464000, People's Republic of China

⁵⁹ Zhejiang University, Hangzhou 310027, People's Republic of China

⁶⁰ Zhengzhou University, Zhengzhou 450001, People's Republic of China

^a Also at Bogazici University, 34342 Istanbul, Turkey

^b Also at the Moscow Institute of Physics and Technology, Moscow 141700, Russia

^c Also at the Functional Electronics Laboratory, Tomsk State University, Tomsk, 634050, Russia

^d Also at the Novosibirsk State University, Novosibirsk, 630090, Russia

^e Also at the NRC "Kurchatov Institute", PNPI, 188300, Gatchina, Russia

^f Also at Istanbul Arel University, 34295 Istanbul, Turkey

^g Also at Goethe University Frankfurt, 60323 Frankfurt am Main, Germany

^h Also at Key Laboratory for Particle Physics, Astrophysics and Cosmology, Ministry of Education; Shanghai Key Laboratory for Particle Physics and Cosmology; Institute of Nuclear and Particle Physics, Shanghai 200240, People's Republic of China

ⁱ Also at Government College Women University, Sialkot - 51310. Punjab, Pakistan.

^j Also at Key Laboratory of Nuclear Physics and Ion-beam Application (MOE) and Institute of Modern Physics, Fudan University, Shanghai 200443, People's Republic of China

(Dated: June 4, 2019)

We study e^+e^- collisions with a $\pi^+\pi^-\pi^0\eta_c$ final state using data samples collected with the BESIII detector at center-of-mass energies $\sqrt{s} = 4.226, 4.258, 4.358, 4.416, \text{ and } 4.600$ GeV. Evidence for the decay $Z_c(3900)^\pm \rightarrow \rho^\pm\eta_c$ is reported with a statistical significance of 3.9σ with various systematic uncertainties taken into account at $\sqrt{s} = 4.226$ GeV, and the Born cross section times branching fraction $\sigma^B(e^+e^- \rightarrow \pi^\mp Z_c(3900)^\pm) \times \mathcal{B}(Z_c(3900)^\pm \rightarrow \rho^\pm\eta_c)$ is measured to be $(48 \pm 11 \pm 11)$ pb. The $Z_c(3900)^\pm \rightarrow \rho^\pm\eta_c$ signal is not significant at the other center-of-mass energies and the corresponding upper limits are determined. In addition, no significant signal is observed in a search for $Z_c(4020)^\pm \rightarrow \rho^\pm\eta_c$ with the same data samples. The ratios $R_{Z_c(3900)} = \mathcal{B}(Z_c(3900)^\pm \rightarrow \rho^\pm\eta_c)/\mathcal{B}(Z_c(3900)^\pm \rightarrow \pi^\pm J/\psi)$ and $R_{Z_c(4020)} = \mathcal{B}(Z_c(4020)^\pm \rightarrow \rho^\pm\eta_c)/\mathcal{B}(Z_c(4020)^\pm \rightarrow \pi^\pm h_c)$ are obtained and used to discriminate between different theoretical interpretations of the $Z_c(3900)^\pm$ and $Z_c(4020)^\pm$.

PACS numbers: 14.40.Rt, 13.66.Bc, 14.40.Pq, 13.25.Gv

The charged charmonium-like states $Z_c(3900)^\pm$ [1–3] and $Z_c(4020)^\pm$ [4, 5] were first observed in 2013. Although their observed properties indicate that they are not conventional mesons consisting of a quark-antiquark pair, their exact quark configurations are still unknown. There are many models developed to interpret their inner structures [6], such as loosely bound hadronic molecules of two charmed mesons [7], compact tetraquarks [8], and hadro-quarkonium [9, 10].

It has recently been suggested that the relative decay rate

of Z_{cS} with the same charge, such as $Z_c^{\pm,0}(3900) \rightarrow \rho^{\pm,0}\eta_c$ to $\pi^{\pm,0}J/\psi$ (or $Z_c^{\pm,0}(4020) \rightarrow \rho^{\pm,0}\eta_c$ to $\pi^{\pm,0}h_c$), can be used to discriminate between the molecule and tetraquark scenarios [11]. In the tetraquark scenario, the predicted ratio of $\mathcal{B}(Z_c(3900) \rightarrow \rho\eta_c)/\mathcal{B}(Z_c(3900) \rightarrow \pi J/\psi)$ is 230 or 0.27, depending on whether or not the spin-spin interaction outside the diquarks is kept. In the meson molecule framework, on the other hand, this ratio is only 0.046. Similarly, the predicted ratio of $\mathcal{B}(Z_c(4020) \rightarrow \rho\eta_c)/\mathcal{B}(Z_c(4020) \rightarrow \pi h_c)$ is 6.6 in the tetraquark model, but only 0.010 in the meson

molecule model [11]. Therefore, a search for the decays of $Z_c(3900)$ or $Z_c(4020)$ to $\rho\eta_c$ offers an important opportunity to understand their internal structure.

In this Letter, we report a search for the charged Z_c decays of $Z_c(3900)^\pm(Z_c(4020)^\pm) \rightarrow \rho^\pm\eta_c$ using the process $e^+e^- \rightarrow \pi^+\pi^-\pi^0\eta_c$. We use data samples collected with the BESIII detector [12] at center-of-mass (c.m.) energies above 4 GeV, as listed in Table I. The integrated luminosities of these data samples are measured by analyzing large-angle Bhabha scattering events with an uncertainty of 1.0% [13], and the c.m. energies are measured using the $e^+e^- \rightarrow \mu^+\mu^-$ process with an uncertainty of ± 0.8 MeV [14]. The η_c is reconstructed from nine hadronic decay modes: $p\bar{p}$, $2(K^+K^-)$, $K^+K^-\pi^+\pi^-$, $K^+K^-\pi^0$, $p\bar{p}\pi^0$, $K_S^0K^\pm\pi^\mp$, $\pi^+\pi^-\eta$, $K^+K^-\eta$, and $\pi^+\pi^-\pi^0\pi^0$. The K_S^0 is reconstructed from its $\pi^+\pi^-$ decay and the η from its $\gamma\gamma$ final state.

The design and performance of the BESIII detector are given in Ref [12]. The GEANT4-based [15] Monte Carlo (MC) simulation software package, which includes the geometric description of the BESIII detector and the detector response, is used to optimize event selection criteria, determine the detection efficiencies, and estimate the backgrounds. The inclusive MC sample consists of generic $\Lambda_c^+\bar{\Lambda}_c^-$ events, $D_{(s)}^{(*)}\bar{D}_{(s)}^{(*)}+X$ production, initial state radiation (ISR) return to charmonium(-like) states at lower masses, and the continuum processes $e^+e^- \rightarrow q\bar{q}(q = u, d, s)$. At each energy, the signal events are generated according to phase space using EVTGEN [16]. The ISR is simulated with KKMC [17], and the maximum ISR photon energy is set according to the production threshold of the $\pi^+\pi^-\pi^0\eta_c$ system. Final state radiation is handled with PHOTOS [18].

Charged tracks are reconstructed from the drift chamber hits within a fiducial range of $|\cos\theta| < 0.93$, where θ is the polar angle of the track. We require that the point of closest approach to the interaction point is within 10 cm in the beam direction and within 1 cm in the plane perpendicular to the beam direction. A vertex fit constrains all the charged tracks to originate from a common point. Since the K_S^0 has a relatively long lifetime, the requirements on the track point of closest approach and the vertex fit are not applied to the pion tracks associated with its decay. For each charged track, the time-of-flight (TOF) and energy-loss dE/dx information is used for Particle identification (PID) to calculate the corresponding probabilities for pion, kaon, and proton hypotheses. These probabilities are combined with information from kinematic fit, described later, to choose among the charged particle hypotheses.

Photon candidates are reconstructed by clustering the electromagnetic calorimeter (EMC) crystal energies. Only clusters with a deposited energy of at least 25 MeV in the barrel region ($|\cos\theta| < 0.8$) or 50 MeV in the endcap region ($0.86 < |\cos\theta| < 0.92$) are accepted. The energy deposited in the nearby TOF counters is included to improve the recon-

struction efficiency and energy resolution. An EMC timing requirement [0, 700] ns is used to suppress electronic noise and energy deposits unrelated to the event.

To reconstruct π^0 and η , the invariant mass of a photon pair is required to be in the range [0.120, 0.145] GeV/ c^2 for π^0 and [0.50, 0.57] GeV/ c^2 for η , which are approximately equivalent to a $\pm 3\sigma$ window around the nominal mass of π^0 or η . To improve the resolution, a one-constraint (1C) kinematic fit is imposed on the selected photon pairs to constrain their invariant mass to the nominal π^0 or η mass [19].

We reconstruct a K_S^0 via its $\pi^+\pi^-$ decay mode. A kinematic constraint between the production and decay vertices, and a secondary vertex fitting algorithm based on the least squares method are both employed [20]. To suppress background, it is required that the ratio of decay length to its uncertainty is greater than two, and the invariant mass of $\pi^+\pi^-$ is within [0.488, 0.508] GeV/ c^2 , which is $\pm 3\sigma$ with respect to the nominal K_S^0 mass [19].

The η_c candidates are reconstructed by the nine hadronic decays mentioned earlier. All combinations with invariant mass in the range [2.7, 3.2] GeV/ c^2 are kept within each event. The signal region for the η_c candidates is defined as [2.95, 3.02] GeV/ c^2 and the sidebands are [2.78, 2.92] and [3.05, 3.19] GeV/ c^2 .

The entire decay sequence is fully reconstructed for each η_c decay channel. After the above selection, a four-constraint (4C) kinematic fit is performed for each event, and the χ^2 of the fit (χ_{4C}^2) is required to be less than 40 to suppress backgrounds. In the kinematic fit, all charged tracks are assigned to the assumed particle species if there is only one type of particle in the final state. Otherwise, each track is assigned to all possible hypotheses. If there is more than one combination in an event, the one with minimum $\chi_{min}^2 \equiv \chi_{4C}^2 + \chi_{1C}^2 + \chi_{PID}^2 + \chi_{vertex}^2$ is kept for further analysis. Here, χ_{1C}^2 is the χ^2 of the 1C fit for π^0 (η), χ_{PID}^2 is the sum of the χ^2 for the PID of all charged tracks, and χ_{vertex}^2 is the χ^2 of the K_S^0 secondary vertex fit.

Inclusive MC samples with the same statistics as the data are studied to understand the backgrounds. The major backgrounds to $e^+e^- \rightarrow \pi^+\pi^-\pi^0\eta_c$ are classified into two categories. They are events from (1) charmonium(-like) states decays (most of which include open-charm decays, e.g. $\psi \rightarrow D^{(*)}\bar{D}^{(*)}$); and (2) the continuum process, $e^+e^- \rightarrow q\bar{q}$, with $q = u, d, s$. It is found that about two thirds of the background events originate from the continuum process, and the rest are from resonance decays.

Background events with charmed mesons are rejected if a D meson candidate is reconstructed in one of its five major decay modes: $D^0 \rightarrow K^\pm\pi^\mp$, $D^0 \rightarrow K^\pm\pi^\mp\pi^0$, $D^\pm \rightarrow K^\pm\pi^\mp\pi^\pm$, $D^\pm \rightarrow K_S^0\pi^\pm$, and $D^\pm \rightarrow K_S^0\pi^\pm\pi^0$. To accomplish this, we require the invariant mass of $D^0(D^\pm)$ candidates to be outside the region $m(D^0) \pm 24$ MeV ($m(D^\pm) \pm 10$ MeV). Events with a $K^*(892) \rightarrow K\pi$, an $\omega \rightarrow \pi^+\pi^-\pi^0$, or an $\eta \rightarrow \pi^+\pi^-\pi^0$ candidate are removed to

reduce the continuum background by requiring $|M(K\pi) - m(K^*)| > 32 \text{ MeV}$, $|M(\pi^+\pi^-\pi^0) - m(\omega)| > 26 \text{ MeV}$, and $|M(\pi^+\pi^-\pi^0) - m(\eta)| > 10 \text{ MeV}$, respectively. Here, $m(D^0)$, $m(D^\pm)$, $m(K^*)$, $m(\omega)$ and $m(\eta)$ are the nominal masses of the corresponding states.

By analyzing 600,000 $e^+e^- \rightarrow \pi^+\pi^-h_c$ MC simulation events with h_c decaying inclusively, a small enhancement in the η_c signal region is found. Its contribution, $N_{\text{bkg}}^{\text{peaking}}$, is estimated to be 8.7 ± 2.0 at $\sqrt{s} = 4.226 \text{ GeV}$ using results from Ref [4]. The contributions at other energies are estimated in a similar way. Except this mode, no peaking background is found.

The mass windows for the background veto and the χ^2 requirement of the 4C kinematic fit are determined by optimizing the figure-of-merit (FOM), which is defined as $\text{FOM} = S/\sqrt{S+B}$. Here, S is the number of signal events from the MC simulation (assuming $\sigma(e^+e^- \rightarrow \pi^+\pi^-\pi^0\eta_c) = 50 \text{ pb}$, which is evaluated from a measurement using unoptimized selection criteria), and B is the number of background events obtained from the η_c sidebands in the data. The optimization is performed through iterations until all the selection criteria become stable.

To obtain the $\pi^+\pi^-\pi^0\eta_c$ yield, the invariant mass distributions of the η_c candidates in the nine decay modes are fitted simultaneously using an unbinned maximum likelihood method. In the fit, both the signal and background shapes are channel dependent but the relative signal yields among all the channels are constrained by branching fractions and efficiencies. The η_c signal is described with a constant width Breit-Wigner function (mass and width are fixed to the world average values [19]) convolved with instrumental resolution determined from the MC simulation. The background is parameterized with a second order Chebyshev Polynomial (CP) function. The total signal yield of the nine channels is N_{obs} , which is shared for all the channels and required to be positive. $N_{\text{obs}} \times f_i$ is the signal yield of the i th channel. Here, the weight factor is $f_i \equiv \varepsilon_i \mathcal{B}_i / \sum_i \varepsilon_i \mathcal{B}_i$, where \mathcal{B}_i denotes the branching fraction of η_c decays to the i th mode [21] and ε_i represents the corresponding efficiency. The free parameters in the fit include N_{obs} and the background parameters for each decay mode. Figure 1(left) shows the fit results at $\sqrt{s} = 4.226 \text{ GeV}$ projected onto the sum of events from all nine η_c decay modes. Figure 1(right) shows the background subtracted distribution. The total signal yield is 333_{-80}^{+83} with a statistical significance of 4.2σ , which is obtained by comparing the change of the log-likelihood value $\Delta(-\ln L) = 9.0$ and degrees of freedom $\Delta\text{dof} = 1$ with and without the $\pi^+\pi^-\pi^0\eta_c$ signal in the fit. The same selection criteria are applied to the data sets at $\sqrt{s} = 4.258, 4.358, 4.416, \text{ and } 4.600 \text{ GeV}$, but no significant signals are observed.

The Born cross section of the $e^+e^- \rightarrow \pi^+\pi^-\pi^0\eta_c$ reaction is calculated using

$$\sigma^{\text{B}}(e^+e^- \rightarrow \pi^+\pi^-\pi^0\eta_c) = \frac{N_{\text{sig}}}{\mathcal{L}(1+\delta) \frac{1}{|1-\Pi|^2} \sum_i \varepsilon_i \mathcal{B}_i}, \quad (1)$$

where $N_{\text{sig}} = N_{\text{obs}} - N_{\text{bkg}}^{\text{peaking}}$ is the number of signal events after the peaking background subtraction; \mathcal{L} is the integrated luminosity; $(1+\delta)$ is the ISR correction factor, assuming the $\pi^+\pi^-\pi^0\eta_c$ signal is from $Y(4260)$ decays [19]; and $\frac{1}{|1-\Pi|^2}$ is the vacuum-polarization factor [22]. The cross sections and the numbers used in its calculation are listed in Table I for all energy points. The upper limits of the cross sections at 90% confidence level (C.L.) are determined using a Bayesian method, assuming a flat prior in σ^{B} . The systematic uncertainties are incorporated into the upper limit by smearing the probability density function of the cross section [23]. The corresponding results for $\sigma_{\text{U.L.}}^{\text{B}}$ are also listed in Table I.

The $Z_c(3900)^\pm$ ($Z_c(4020)^\pm$) signals are examined after requiring that the invariant mass of an η_c candidate is within the η_c signal region [2.95, 3.02] GeV/c^2 and the invariant mass of $\pi^\pm\pi^0$ is within the ρ signal region [0.675, 0.875] GeV/c^2 . Here, all possible combinations in one event are kept to avoid bias. To suppress the combinatorial background, the momenta of the pions from ρ decays are required to be less than 0.8 GeV/c . The events in the η_c and ρ sidebands are used to estimate the background. The recoil mass spectrum of the remaining π^\mp is shown in Fig. 2 for the data at $\sqrt{s} = 4.226 \text{ GeV}$, together with the contribution from the η_c and ρ sideband events. Here, the ρ sideband is defined as [0.475, 0.675] GeV/c^2 . In Fig. 2, the $Z_c(3900)^\pm$ signal is apparent, but there is no statistically significant $Z_c(4020)^\pm$ signal.

To obtain the yields of $e^+e^- \rightarrow \pi^\mp Z_c(3900)^\pm \rightarrow \pi^\mp \rho^\pm \eta_c$ and $e^+e^- \rightarrow \pi^\mp Z_c(4020)^\pm \rightarrow \pi^\mp \rho^\pm \eta_c$, the invariant masses of $\rho^\pm \eta_c$ candidates in the nine η_c decay channels are fitted simultaneously using the same method as for $e^+e^- \rightarrow \pi^+\pi^-\pi^0\eta_c$. In the fit, a possible interference between the signal and the background is neglected. The mass and width of the $Z_c(3900)^\pm$ are fixed to the values from the latest measurement [24] and those of the $Z_c(4020)^\pm$ are fixed to world average values [19]. The mass resolution is obtained from MC simulation and parameterized as a Crystal Ball function [25]. The background is described with a second order CP function. Figure 2(left) shows the fit to the invariant mass of $\rho^\pm \eta_c$ summed over the nine η_c decays at $\sqrt{s} = 4.226 \text{ GeV}$. Figure 2(right) is the background subtracted distribution. The total $Z_c(3900)^\pm$ signal yield is 240_{-54}^{+56} events with a statistical significance of 4.3σ , and that of the $Z_c(4020)^\pm$ is 21_{-11}^{+15} events with a statistical significance of 1.0σ . The signals at the other c.m. energies are not statistically significant.

The Born cross section for $e^+e^- \rightarrow \pi^\mp Z_c^\pm$ with $Z_c^\pm \rightarrow \rho^\pm \eta_c$ is calculated using

$$\sigma^{\text{B}}(e^+e^- \rightarrow \pi^\mp Z_c^\pm \rightarrow \rho^\pm \eta_c) = \frac{N_{\text{obs}}^{Z_c}}{\mathcal{L}(1+\delta) \frac{1}{|1-\Pi|^2} \sum_i \varepsilon_i^{Z_c} \mathcal{B}_i}, \quad (2)$$

where $N_{\text{obs}}^{Z_c}$ is the total signal yield of the Z_c and $\varepsilon_i^{Z_c}$ is the corresponding detection efficiency. The definitions of other factors are the same as in Eq. (1). The numbers used in the calculation and the results are listed in Table II.

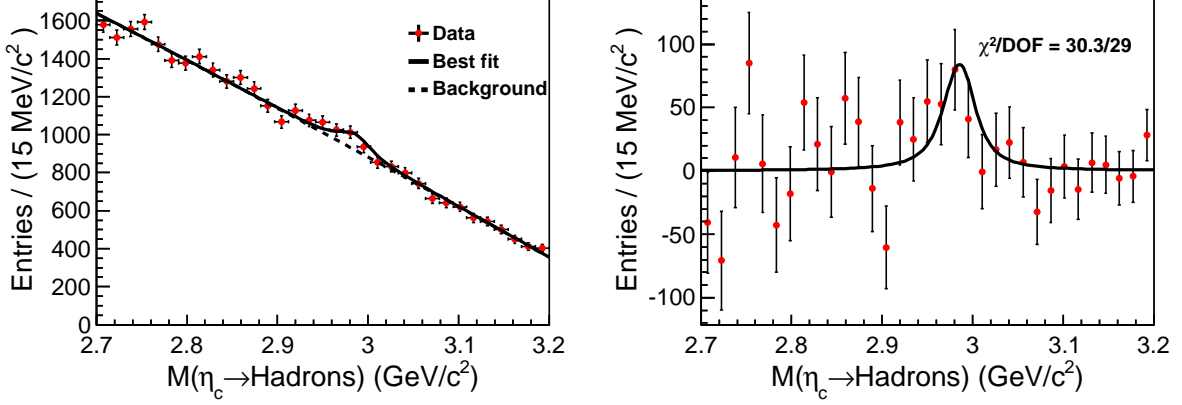


FIG. 1. Invariant mass distributions of the η_c candidates summed over nine channels in $e^+e^- \rightarrow \pi^+\pi^-\pi^0\eta_c$ at $\sqrt{s} = 4.226$ GeV (left panel), and the signal after background subtraction (right panel). Dots with error bars are the data, solid lines are the total fit and the dotted line is background.

TABLE I. The Born cross section (σ^B) for the $e^+e^- \rightarrow \pi^+\pi^-\pi^0\eta_c$ process and the numbers that enter the calculation (see Eq. (1)). $\sigma_{U.L.}^B$ is the upper limit of the cross section at the 90% C.L., and S is the statistical significance of the signal.

\sqrt{s} (GeV)	\mathcal{L} (pb $^{-1}$)	N_{obs}	$(1 + \delta)$	$\frac{1}{ 1 - \Pi ^2}$	$\sum \varepsilon_i \mathcal{B}_i$ (%)	σ^B (pb)	$\sigma_{U.L.}^B$ (pb)	S (σ)
4.226	1091.7	333_{-80}^{+83}	0.74	1.056	0.82	$46_{-11}^{+12} \pm 10$	< 78	4.2
4.258	825.7	161_{-68}^{+73}	0.76	1.054	0.80	$30_{-13}^{+14} \pm 9$	< 67	2.4
4.358	539.8	37_{-24}^{+62}	1.03	1.051	0.62	$9_{-7}^{+17} \pm 2$	< 41	...
4.416	1073.6	27_{-18}^{+82}	1.15	1.053	0.49	$3_{-3}^{+13} \pm 1$	< 38	...
4.600	566.9	0_{-0}^{+28}	1.32	1.055	0.31	$0_{-0}^{+12} \pm 13$	< 36	...

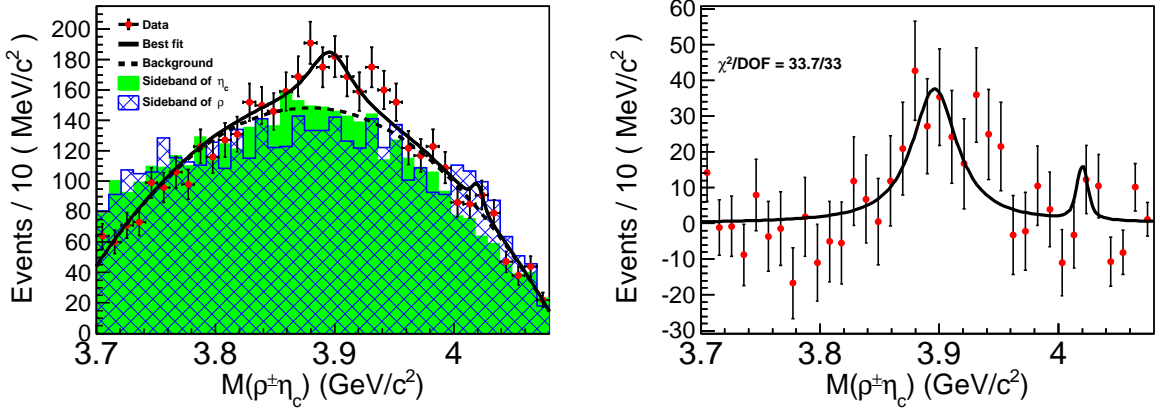


FIG. 2. The $\rho^\pm\eta_c$ invariant mass distribution summed over nine η_c decay channels in $e^+e^- \rightarrow \pi^\mp\rho^\pm\eta_c$ at $\sqrt{s} = 4.226$ GeV and fit with $Z_c(3900)^\pm$ and $Z_c(4020)^\pm$ signals (left panel); and the same plot with background subtracted (right panel). Dots with error bars are data, the shaded histogram is from η_c sidebands, and the shaded histogram with grid lines is from the ρ sideband. Both are normalized to the number of background events from the fit. The solid lines are the total fit and the dotted line is the background.

TABLE II. Born cross sections of $e^+e^- \rightarrow \pi^\mp Z_c(3900)^\pm (Z_c(4020)^\pm) \rightarrow \pi^\mp\rho^\pm\eta_c$ (numbers for $Z_c(4020)^\pm$ are in brackets). The parameters are defined in the same way as those in Table I.

\sqrt{s} (GeV)	$N_{\text{obs}}^{Z_c}$	$(1 + \delta)$	$\frac{1}{ 1 - \Pi ^2}$	$\sum \varepsilon_i^{Z_c} \mathcal{B}_i$ (%)	σ^B (pb)	$\sigma_{U.L.}^B$ (pb)	S (σ)
4226.3	$240_{-54}^{+56} (21_{-11}^{+15})$	0.74	1.056	0.59 (0.52)	$48_{-11}^{+11} \pm 11$	< 78 (14)	4.3 (1.0)
4258.0	$92_{-43}^{+48} (0_{-0}^{+11})$	0.76	1.054	0.50 (0.56)	$28_{-13}^{+15} \pm 8$	< 62 (6)	2.0 (...)
4358.3	$12_{-8}^{+40} (0_{-0}^{+15})$	1.03	1.051	0.44 (0.42)	$5_{-3}^{+16} \pm 2$	< 36 (14)	0.3 (...)
4415.6	$101_{-44}^{+48} (6_{-4}^{+17})$	1.15	1.053	0.35 (0.34)	$22_{-10}^{+10} \pm 5$	< 44 (11)	2.2 (...)
4599.5	$0_{-0}^{+11} (0_{-0}^{+10})$	1.32	1.055	0.20 (0.21)	$0_{-0}^{+7} \pm 1$	< 14 (21)	...

The systematic uncertainties in the $\sigma^{\text{B}}(e^+e^- \rightarrow \pi^+\pi^-\pi^0\eta_c)$ measurement originate from the uncertainty of each factor in Eq. (1). The integrated luminosity has an uncertainty of 1.0% [13]. The number of $e^+e^- \rightarrow \pi^+\pi^-h_c$, $h_c \rightarrow \gamma\eta_c$ peaking background events is estimated with MC simulation of $e^+e^- \rightarrow \pi^+\pi^-h_c$, so both the cross section uncertainty and the statistical error of the peaking background from the MC sample are taken into account to estimate this uncertainty. For the ISR correction, we assume that the $e^+e^- \rightarrow \pi^+\pi^-\pi^0\eta_c$ events mainly come from the $Y(4260)$. Alternatively, the c.m. energy dependent cross section of $e^+e^- \rightarrow \pi^+\pi^-J/\psi$ measured by the BESIII experiment [26] is used to estimate this uncertainty. The uncertainty from the signal shape consists of the mass resolution discrepancy between data and MC simulation and the uncertainty of the η_c resonant parameters. The former is studied using an $e^+e^- \rightarrow \gamma_{\text{ISR}}J/\psi$ [27] sample and the latter is estimated by varying the η_c parameters by $\pm 1\sigma$ around the world average values [19]. The uncertainty for the background shape is estimated by changing the order of the CP function. The uncertainty in the fitting range is obtained by adjusting the boundaries. The methods to estimate the uncertainties due to the vacuum polarization and $\sum_i \varepsilon_i \mathcal{B}_i$ are the same as described in Ref. [23]. Furthermore, when we estimate the uncertainty of $\sum_i \varepsilon_i \mathcal{B}_i$, the uncertainty due to the $e^+e^- \rightarrow \pi^+\pi^-\pi^0\eta_c$ decay dynamics is obtained by comparing the simulations with and without the Z_c resonance. All of the sources are assumed to be independent and added in quadrature and the largest contribution to the systematics is the uncertainty of $\sum_i \varepsilon_i \mathcal{B}_i$. The total systematic uncertainties are listed in Table I.

For the $\sigma^{\text{B}}(e^+e^- \rightarrow \pi^\mp Z_c(3900)^\pm(Z_c(4020)^\pm) \rightarrow \pi^\mp \rho^\pm \eta_c)$ measurement, the uncertainties on \mathcal{L} , ISR factors, $\sum \varepsilon \mathcal{B}$ and the vacuum polarization factor are studied following the methods described in the measurement of $\sigma^{\text{B}}(e^+e^- \rightarrow \pi^+\pi^-\pi^0\eta_c)$. Moreover, additional sources of systematic uncertainties come from the ρ and η_c selections, and the fit to the $Z_c(3900)^\pm(Z_c(4020)^\pm)$ resonances. The uncertainty due to the $M(\pi^\pm\pi^0)$ mass window is estimated by comparing the invariant mass of $M(\omega \rightarrow \pi^+\pi^-\pi^0)$ in data and MC assuming the mass resolution of $M(\pi^+\pi^-\pi^0)$ is larger than $M(\pi^\pm\pi^0)$. The discrepancy is found to be negligible. The uncertainty of the η_c line shape is estimated by the variation of the mass and width of the η_c within the errors given by world average values [19]. The uncertainties due to the fit to the $Z_c(3900)^\pm(Z_c(4020)^\pm)$ are estimated with the same methods as in the $\pi^+\pi^-\pi^0\eta_c$ case. All these sources and those in the $\sigma^{\text{B}}(e^+e^- \rightarrow \pi^+\pi^-\pi^0\eta_c)$ measurement (except the uncertainties of the fit) are assumed to be independent and added in quadrature, and the total systematic uncertainties are listed in Table II. To consider the effect of the systematic uncertainty on the signal significance at $\sqrt{s} = 4.226$ GeV, we vary the signal shape, background parametrization, and fit range, or free the Z_c mass in the fit. We find the statistical significance of the $Z_c(3900)$ is always larger than 3.9σ in all the checks.

In summary, we report the first evidence for the $\rho\eta_c$ de-

cay mode of the charged charmonium-like state $Z_c(3900)^\pm$ in the e^+e^- annihilation data at $\sqrt{s} = 4.226$ GeV, and measure the cross section times branching ratio $\sigma^{\text{B}}(e^+e^- \rightarrow \pi^\mp Z_c(3900)^\pm) \times \mathcal{B}(Z_c(3900)^\pm \rightarrow \rho^\pm \eta_c) = (48 \pm 11 \pm 11)$ pb. This result is very close to the cross section of $e^+e^- \rightarrow \pi^+\pi^-\pi^0\eta_c$, which is $(46_{-11}^{+12} \pm 10)$ pb. This indicates that the $e^+e^- \rightarrow \pi^+\pi^-\pi^0\eta_c$ process is dominated by the process $e^+e^- \rightarrow \pi^\mp Z_c(3900)^\pm \rightarrow \pi^\mp \rho^\pm \eta_c$. The statistical significance of $Z_c(3900)^\pm \rightarrow \rho^\pm \eta_c$ is 4.3σ (3.9σ including the systematical uncertainty). No signal is observed at $\sqrt{s} = 4.258, 4.358, 4.416,$ and 4.600 GeV and the upper limits of the production cross sections at 90% C.L. are determined. No significant signal of $Z_c(4020)^\pm \rightarrow \rho^\pm \eta_c$ is found in any of the data sets and the upper limits of the production cross sections are determined.

Using the results from Refs. [4] and [24], we calculate the ratios $R_{Z_c(3900)} = \mathcal{B}(Z_c(3900)^\pm \rightarrow \rho^\pm \eta_c) / \mathcal{B}(Z_c(3900)^\pm \rightarrow \pi^\pm J/\psi)$ and $R_{Z_c(4020)} = \mathcal{B}(Z_c(4020)^\pm \rightarrow \rho^\pm \eta_c) / \mathcal{B}(Z_c(4020)^\pm \rightarrow \pi^\pm h_c)$. The results at $\sqrt{s} = 4.226, 4.258,$ and 4.358 GeV are listed in Table III, together with the theoretical predictions from Ref. [11] for comparison.

The measured $R_{Z_c(3900)}$ is closer to the calculation of the tetraquark model than that of the molecule model [11]. The measurement is also consistent with several other independent calculations based on the tetraquark scenario [28–31]. As for the molecule model, we notice that the calculated $R_{Z_c(3900)}$ is highly model dependent and varies from 6.7×10^{-3} to 1.8 in different approaches [31–35]. Therefore, it is necessary to narrow down the theoretical uncertainty in the molecular framework to have a better comparison with the measurement. In the hadron-charmonium model, the $\mathcal{B}(Z_c(3900) \rightarrow \rho\eta_c)$ is suppressed compared with $\mathcal{B}(Z_c(3900) \rightarrow \pi J/\psi)$ and therefore inconsistent with the measurement [36]. Furthermore, this model predicts a new resonance $W_c(3785)$, which can be produced via $e^+e^- \rightarrow \rho W_c \rightarrow \rho\pi\eta_c$, the same final state we analyzed here. As we found that the $e^+e^- \rightarrow \pi^+\pi^-\pi^0\eta_c$ process is saturated by the $e^+e^- \rightarrow \pi Z_c(3900) \rightarrow \rho\pi\eta_c$, the production of the W_c is minor compared with $e^+e^- \rightarrow \pi Z_c(3900)$ if it exists.

For $R_{Z_c(4020)}$, we can only report upper limits, but it is smaller than the calculations based on the tetraquark model. Meanwhile, it is not in contradiction with the molecule model calculation, which is about two orders of magnitude smaller than the current upper limit [11].

The BESIII collaboration thanks the staff of BEPCII and the IHEP computing center for their strong support. This work is supported in part by National Key Basic Research Program of China under Contract No. 2015CB856700; National Natural Science Foundation of China (NSFC) under Contracts Nos. 11335008, 11425524, 11625523, 11635010, 11735014; the Chinese Academy of Sciences (CAS) Large-Scale Scientific Facility Program; the CAS Center for Excellence in Particle Physics (CCEPP); Joint Large-Scale Scientific Facility Funds

TABLE III. Comparison of the measured $R_{Z_c(3900)}$ and $R_{Z_c(4020)}$ with the theoretical predictions from Ref. [11]. “Type-I” and “Type-II” represent the tetraquark model predictions with and without taking into account the spin-spin interaction outside the diquarks, and “Molecule” is the molecule model prediction.

	$\sqrt{s} = 4.226 \text{ GeV}$	$\sqrt{s} = 4.258 \text{ GeV}$	$\sqrt{s} = 4.358 \text{ GeV}$	Type-I	Type-II	Molecule
$R_{Z_c(3900)}$	2.2 ± 0.9	< 5.6	...	230^{+330}_{-140}	$0.27^{+0.40}_{-0.17}$	$0.046^{+0.025}_{-0.017}$
$R_{Z_c(4020)}$	< 1.6	< 0.9	< 1.4	$6.6^{+56.8}_{-5.8}$		$0.010^{+0.006}_{-0.004}$

of the NSFC and CAS under Contracts Nos. U1532257, U1532258, U1732263; CAS Key Research Program of Frontier Sciences under Contracts Nos. QYZDJ-SSW-SLH003, QYZDJ-SSW-SLH040; 100 Talents Program of CAS; IN-PAC and Shanghai Key Laboratory for Particle Physics and Cosmology; German Research Foundation DFG under Contracts Nos. Collaborative Research Center CRC 1044, FOR 2359; Istituto Nazionale di Fisica Nucleare, Italy; Koninklijke Nederlandse Akademie van Wetenschappen (KNAW) under Contract No. 530-4CDP03; Ministry of Development of Turkey under Contract No. DPT2006K-120470; National Science and Technology fund; The Swedish Research Council; U. S. Department of Energy under Contracts Nos. DE-FG02-05ER41374, DE-SC-0010118, DE-SC-0010504, DE-SC-0012069; University of Groningen (RuG) and the Helmholtzzentrum fuer Schwerionenforschung GmbH (GSI), Darmstadt.

- [1] M. Ablikim *et al.* [BESIII Collaboration], Phys. Rev. Lett. **110**, 252001 (2013).
- [2] Z. Q. Liu *et al.* [Belle Collaboration], Phys. Rev. Lett. **110**, 252002 (2013).
- [3] M. Ablikim *et al.* [BESIII Collaboration], Phys. Rev. Lett. **112**, 022001 (2014).
- [4] M. Ablikim *et al.* [BESIII Collaboration], Phys. Rev. Lett. **111**, 242001 (2013).
- [5] M. Ablikim *et al.* [BESIII Collaboration], Phys. Rev. Lett. **112**, 132001 (2014).
- [6] For recent reviews, see H. X. Chen, W. Chen, X. Liu and S. L. Zhu, Phys. Rept. **639**, 1 (2016); N. Brambilla *et al.*, Eur. Phys. J. C **71**, 1534 (2011).
- [7] M. B. Voloshin and L. B. Okun, JETP Lett. **23**, 333 (1976) [Pisma Zh. Eksp. Teor. Fiz. **23**, 369 (1976)].
- [8] L. Maiani, F. Piccinini, A. D. Polosa and V. Riquer, Phys. Rev. D **71**, 014028 (2005).
- [9] M. B. Voloshin, Prog. Part. Nucl. Phys. **61**, 455 (2008).
- [10] S. Dubynskiy and M. B. Voloshin, Phys. Lett. B **666**, 344 (2008).
- [11] A. Esposito, A. L. Guerrieri and A. Pilloni, Phys. Lett. B **746**, 194 (2015).
- [12] M. Ablikim *et al.* [BESIII Collaboration], Nucl. Instrum. Meth. A **614**, 345 (2010).
- [13] M. Ablikim *et al.* [BESIII Collaboration], Chin. Phys. C **39**, 093001 (2015).
- [14] M. Ablikim *et al.* [BESIII Collaboration], Chin. Phys. C **40**, 063001 (2016).
- [15] S. Agostinelli *et al.* [GEANT4 Collaboration], Nucl. Instrum. Methods A **506**, 250 (2003).
- [16] D. J. Lange, Nucl. Instrum. Methods Phys. Res., Sect. A **462**, 152 (2001).
- [17] S. Jadach, B. F. L. Ward, and Z. Was, Comput. Phys. Commun. **130**, 260 (2000); Phys. Rev. D **63**, 113009 (2001).
- [18] P. Golonka, and Z. Was, Eur. Phys. J. C **45**, 97 (2006).
- [19] M. Tanabashi *et al.* [Particle Data Group], Phys. Rev. D **98**, 030001 (2018).
- [20] M. Xu, *et al.*, Chin. Phys. C **33**, 428 (2009).
- [21] M. Ablikim *et al.* [BESIII Collaboration], Phys. Rev. D **86**, 092009 (2012).
- [22] F. Jegerlehner, Z. Phys. C **32**, 195 (1986).
- [23] M. Ablikim *et al.* [BESIII Collaboration], Phys. Rev. D **96**, 012001 (2017).
- [24] M. Ablikim *et al.* [BESIII Collaboration], Phys. Rev. Lett. **119**, 072001 (2017).
- [25] M. Oreglia, SLAC Stanford - SLAC-236 (80,REC.APR. 81) 226p.
- [26] M. Ablikim *et al.* [BESIII Collaboration], Phys. Rev. Lett. **118**, 092001 (2017).
- [27] M. Ablikim *et al.* [BESIII Collaboration], Phys. Rev. D **96**, 051101 (2017).
- [28] L. Maiani, V. Riquer, R. Faccini, F. Piccinini, A. Pilloni and A. D. Polosa, Phys. Rev. D **87**, 111102 (2013).
- [29] S. S. Agaev, K. Azizi and H. Sundu, Phys. Rev. D **93**, 074002 (2016).
- [30] J. M. Dias, F. S. Navarra, M. Nielsen and C. M. Zanetti, Phys. Rev. D **88**, 016004 (2013).
- [31] F. Goerke, T. Gutsche, M. A. Ivanov, J. G. Korner, V. E. Lyubovitskij and P. Santorelli, Phys. Rev. D **94**, 094017 (2016).
- [32] S. Patel, M. Shah, K. Thakkar and P. C. Vinodkumar, PoS Hadron **2013**, 189 (2013).
- [33] H. W. Ke, Z. T. Wei and X. Q. Li, Eur. Phys. J. C **73**, 2561 (2013).
- [34] G. Li, X. H. Liu and Z. Zhou, Phys. Rev. D **90**, 054006 (2014).
- [35] Y. Dong, A. Faessler, T. Gutsche and V. E. Lyubovitskij, Phys. Rev. D **88**, 014030 (2013).
- [36] M. B. Voloshin, Phys. Rev. D **87**, 091501 (2013).